

Pair production by Schwinger and Breit-Wheeler processes in bi-frequent fields

A. Otto^{1†}, T. Nusch¹, D. Seipt², B. Kämpfer¹,
D. Blaschke^{3,4,5}, A. D. Panferov⁶, S. A. Smolyansky⁶, A. I. Titov⁴

1 Institute of Radiation Physics, Helmholtz-Zentrum Dresden-Rossendorf,
Bautzner Landstraße 400, 01328 Dresden, Germany
Institut für Theoretische Physik, Technische Universität Dresden,
Zellescher Weg 17, 01062 Dresden, Germany

2 Helmholtz-Institut Jena, Fröbelstieg 3, 07743 Jena, Germany
Theoretisch-Physikalisches Institut, Friedrich-Schiller-Universität Jena,
Max-Wien-Platz 1, 07743 Jena, Germany

3 Institute for Theoretical Physics, University of Wrocław,
pl. M. Borna 9, 50-204 Wrocław, Poland

4 Bogoliubov Laboratory for Theoretical Physics, JINR Dubna,
Joliot-Curie str. 6, 141980 Dubna, Russia

5 National Research Nuclear University (MEPhI), Kashirskoe Shosse 31,
115409 Moscow, Russia

6 Department of Physics, Saratov State University, 410071 Saratov, Russia

(Received 4 April 2016)

Counter-propagating and suitably polarized light (laser) beams can provide conditions for pair production. Here, we consider in more detail the following two situations: (i) In the homogeneity regions of anti-nodes of linearly polarized ultra-high intensity laser beams, the Schwinger process is dynamically assisted by a second high-frequency field, e.g. by a XFEL beam. (ii) A high-energy probe photon beam colliding with a superposition of co-propagating intense laser and XFEL beams gives rise to the laser assisted Breit-Wheeler process. Prospects of such bi-frequent field constellations with respect to the feasibility of conversion of light into matter are discussed.

1. Introduction

The Schwinger effect (Sauter 1931; Schwinger 1951) means the instability of a spatially homogeneous, purely electric field with respect to the decay into a state with pairs, e.g. electrons (e^-) and positrons (e^+), and a screened electric field, symbolically $|\mathbf{E}\rangle \rightarrow |\mathbf{E}'e^+e^-\rangle$ (cf. (Gelis & Tanji 2015) for a recent review). The pair creation rate $w \propto \exp\{-\pi E_c/|\mathbf{E}|\}$ for fields attainable presently in mesoscopic laboratory installations is exceedingly small since the Sauter-Schwinger (critical) field strength $E_c = m^2/|e| = 1.3 \times 10^{18}$ V/m is for electrons/positrons with masses m and charges $\pm e$ so large (we employ here natural units with $c = \hbar = 1$). The notion of dynamical Schwinger process refers to a situation where the spatially homogeneous electric field has a time dependence, $\mathbf{E}(t)$. The particular case of a periodic field is dealt with in (Brezin & Itzykson 1970) with the motivation that tightly focused laser beams can provide high field strengths, e.g. in the anti-nodes of pair-wise counter propagating, linearly polarized beams. The superposition of many laser beams, as considered, e.g. in (Narozhny *et al.* 2004), can enlarge the pair yield noticeably. A particular variant is the superposition of strong

† Email address for correspondence: a.otto@hzdr.de

laser beams and weaker but high-frequency beams which may be idealized as a common classical background field $\mathbf{E}(t) = \mathbf{E}_1(\omega t) + \mathbf{E}_2(N\omega t)$. If the frequency of the second field, $N\omega$ is sufficiently large, the tunneling path through the positron-electron gap is shortened by the assistance of the multi-photon effect (Schützhold *et al.* 2008; Dunne *et al.* 2009) and, as a consequence, the pair production is enhanced. This dynamically assisted Schwinger process supposes a Keldysh parameter $\gamma_1 = (E_c/E_1)(\omega/m) \ll 1$ to stay in the tunneling regime[‡]. The combination $\gamma_1 < 1$ and $\gamma_2 = (E_c/E_2)(N\omega/m) > 1$ is dubbed assisted dynamical Schwinger effect since the field “1” with parameters E_1 , ω refers to the dynamical Schwinger effect in the nomenclature of (Brezin & Itzykson 1970), and the field “2” with parameters E_2 , $N\omega$ is assisting. Various pulse shapes for $E_{1,2}$ have been studied with the goal to seek for optimal combinations (Hebenstreit & Fillion-Gourdeau 2014; Kohlfürst *et al.* 2013; Akal *et al.* 2014). Current lasers reach intensities of 2×10^{22} W/cm² (cf. (Di Piazza *et al.* 2012) for an overview) corresponding to an inverse Keldysh parameter of $\gamma^{-1} = 10$. Planned facilities are, for example, ELI-NP (ELI 2015) and Apollon (Zou *et al.* 2015) (10 PW, 10^{22} W/cm²) or HiPER (HiPER 2015) (100 PW, 10^{26} W/cm²). (The Sauter-Schwinger field strength requires an intensity of 4×10^{29} W/cm².)

All these investigations aim at verifying the decay of the vacuum. Besides the mentioned strong (but presently not strong enough) fields also the Coulomb fields accompanying heavy and super-heavy atomic nuclei have been considered as an option to study the vacuum break down (Rafelski *et al.* 1978, 1971; Müller *et al.* 1972, 1973; Bialynicki-Birula *et al.* 1991). Previous experiments, however, have not been conclusive (Heinz *et al.* 2000).

Another avenue for pair creation is the conversion of light into matter in the collision of photon beams. The Breit-Wheeler process (Breit & Wheeler 1934) refers to the reaction $\gamma' + \gamma \rightarrow e^+ + e^-$ which is a crossing channel of the Compton process or the time-reversed annihilation. The famous experiment E-144 at SLAC (Burke *et al.* 1997) can be interpreted as a two-step process with Compton backscattering of a laser beam and subsequent reaction of the Compton backscattered photons with the laser beam in non-linear Breit-Wheeler pair production (Burke *et al.* 1997; Bamber *et al.* 1999). The notion non-linear Breit-Wheeler process means the instantaneous reaction with a multiple of laser beam photons, i.e. $\gamma' + n\omega_L \rightarrow e^+ + e^-$. Also here one can ask whether the laser assisted non-linear Breit-Wheeler process $\gamma' + \omega_{XFEL} + n\omega_L \rightarrow e^+ + e^-$ shows peculiarities due to the superposition of the co-propagating XFEL and laser beams.

Other field combinations, such as the nuclear Coulomb field and XFEL/laser beams, are also conceivable (Augustin & Müller 2014; Di Piazza *et al.* 2010) (cf. (Di Piazza *et al.* 2012) for a recent review and further references), but will not be addressed here.

Our paper is organized as follows. In section 2 we consider the reasoning for forming resonance type structures in the phase space distribution of pairs created in the assisted dynamical Schwinger process. The considered classical background field configuration has been characterized above: the superposition of two spatially homogeneous fields of different strengths and frequencies with a common envelope, as investigated in (Otto *et al.* 2015*a,b*; Panferov *et al.* 2015). Examples are given for the mutual amplification, and some glimpses on the time evolution in simple pulses are provided too. Section 3 deals with the laser assisted Breit-Wheeler process, where spectral caustics have identified already in (Nousch *et al.* 2016). Specifically, we show here the sensitivity of the spectral

[‡] Similar to ionization in atomic physics, one can also for pair production distinguish between a tunneling ($\gamma \ll 1$) and a multi-photon regime ($\gamma \gg 1$), depending on the value of the Keldysh parameter γ .

caustics on the laser beam intensity which is important for multi-shot experiments with not perfectly tuneable intensity parameter. Our approach here utilizes the common XFEL + laser field again as a classical background field to be dealt with in the Furry picture, while the probe photon γ' refers to a quantized radiation field. We briefly summarize in Section 4.

2. Assisted dynamical Schwinger process

In this section we consider pair production in the spirit of the Schwinger process, i.e. creation of e^\pm pairs by a purely electric background field which is assumed to be spatially homogeneous. In the following, we use the notation and formalism as introduced in (Otto *et al.* 2015a). The quantum kinetic equation (Schmidt *et al.* 1998)

$$\dot{f}(\mathbf{p}, t) = \frac{\lambda(\mathbf{p}, t)}{2} \int_{-\infty}^t dt' \lambda(\mathbf{p}, t') (1 - 2f(\mathbf{p}, t')) \cos \theta(\mathbf{p}, t, t') \quad (2.1)$$

determines the time (t) evolution of the dimensionless phase space distribution function per spin projection degree of freedom $\dagger\dagger$ $f(\mathbf{p}, t) = dN(\mathbf{p}, t)/d^3p d^3x$, where N refers to the particle number and d^3p and d^3x are the three dimensional volume elements in momentum (p) and configuration (x) spaces. We emphasize that only $f(\mathbf{p}, t \rightarrow +\infty)$ can be considered as single particle distribution which may represent the source term of a subsequent time evolution of the emerging e^+e^- plasma. The initial condition for solving (2.1) is $f(\mathbf{p}, t \rightarrow -\infty) = 0$. Screening and backreaction are not included with virtue of the small values of f in subcritical fields (cf. (Gelis & Tanji 2013) for recent work on that issue). Above the quantities $\lambda(\mathbf{p}, t) = \frac{eE(t)\varepsilon_\perp(p_\perp)}{\varepsilon^2(\mathbf{p}, t)}$ stand for the amplitude of the vacuum transition, and $\theta(\mathbf{p}, t, t') = 2 \int_{t'}^t d\tau \varepsilon(\mathbf{p}, \tau)$ for the dynamical phase, describing the vacuum oscillations modulated by the external field; the quasi-energy ε , the transverse energy ε_\perp and the longitudinal quasi-momentum P are defined as $\varepsilon(\mathbf{p}, t) = \sqrt{\varepsilon_\perp^2(p_\perp) + P^2(p_\parallel, t)}$ and $\varepsilon_\perp(p_\perp) = \sqrt{m^2 + p_\perp^2}$, $P(p_\parallel, t) = p_\parallel - eA(t)$, where $p_\perp = |\mathbf{p}_\perp|$ is the modulus of the kinetic momentum (\mathbf{p}) component of positrons (electrons) perpendicular to the electric field, and p_\parallel denotes the E -parallel kinetic momentum component. The electric field follows from the potential

$$A = K(\omega t) \left(\frac{E_1}{\omega} \cos(\omega t) + \frac{E_2}{N\omega} \cos(N\omega t) \right) \quad (2.2)$$

by $E = -\dot{A}$ in Coulomb gauge. Equation (2.2) describes a bi-frequent field with frequency ratio N (integer) and field strengths E_1 – the strong field “1” – and E_2 – the weak field “2”. The quantity K is the common envelope function with the properties (i) absolutely flat in the flat-top time interval $-t_{\text{f.t.}}/2 < t < +t_{\text{f.t.}}/2$ and (ii) absolutely zero for $t < -t_{\text{f.t.}}/2 - t_{\text{ramp}}$ and $t > t_{\text{f.t.}}/2 + t_{\text{ramp}}$ and (iii) absolutely smooth everywhere, i.e. K belongs to the C^∞ class; t_{ramp} is the ramping duration characterizing the switching on/off time intervals.

Figure 1 (top row) exhibits three examples for the transverse phase space distribution $f(p_\perp, p_\parallel = 0, t \rightarrow \infty)$ for $E_1 = 0.1 E_c$, $E_2 = 0.05 E_c$, $\omega = 0.02 m$, $N = 25$, $t_{\text{ramp}} = 5 \omega^{-1}$ and $t_{\text{f.t.}} = 25 \omega^{-1}$ obtained by numerically solving Eq. (2.1). The chosen parameters are by far not yet in reach at present and near-future facilities. Due to the periodicity of the

$\dagger\dagger$ In (Otto *et al.* 2015a,b) we employ a different convention with a sum over spin degrees of freedom, i.e. $f \rightarrow \sum_s f$ which removes factors 2 in front of f .

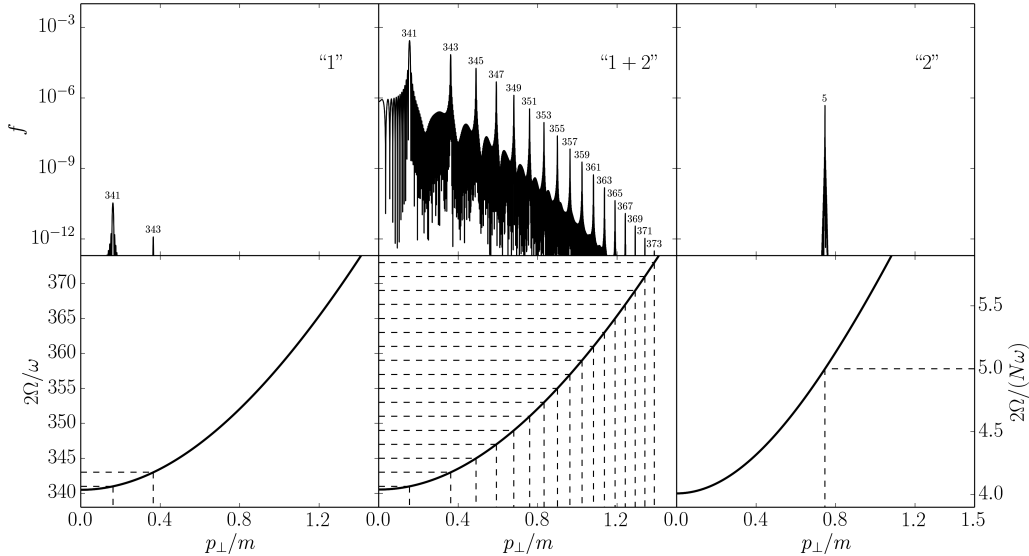


FIGURE 1. Top row: Asymptotic transverse momentum (p_{\perp}) spectrum at $p_{\parallel} = 0$ for the bi-frequent field (2.2) (middle panel) and the field components “1” (left panel, $E_1 = 0.1 E_c$, $\omega = 0.02 m$) and “2” (right panel, $E_2 = 0.05 E_c$, $N = 25$) alone. Bottom row: Fourier zero-modes $2\Omega(p_{\perp}, p_{\parallel} = 0)$ scaled by ω (left and middle panels) and $N\omega$ (right panel) for the fields in the top row with resonance conditions (horizontal dashed lines for $\ell = 341$ and 343 (left; higher- ℓ resonances are not depicted since the peaks are underneath the scale displayed in the top panel), $\ell = 341, \dots, 373$ (middle) and $\ell = 5$ (right); vertical dashed lines are for the resonance positions; peaks for even ℓ appear only for $p_{\parallel} \neq 0$ but get a zero amplitude at $p_{\parallel} = 0$, and thus their positions are not depicted).

involved fields and their finite duration a pronounced peak structure emerges (the peaks become sharp, elliptically bend ridges with deep notches when continuing the spectrum to finite values of p_{\parallel}). The peak heights scale with $t_{\text{f.t.}}^2$, for not too long pulse duration. The peak positions are determined by the resonance condition (Otto *et al.* 2015a)

$$2\Omega(p_{\perp}, p_{\parallel}) - \ell\omega = 0, \quad (2.3)$$

where $\Omega = \frac{m}{2\pi} \int_0^{2\pi} dx \sqrt{1 + (p_{\perp}/m)^2 + [(p_{\parallel}/m) - \gamma_1^{-1} \cos x - \gamma_2^{-1} \cos Nx]^2}$ is the Fourier zero-mode of ε . The values of ℓ (integer) where the resonance condition (2.3) is fulfilled can be used to label the peaks. $\Omega(p_{\perp} = p_{\parallel} = 0)$ may be interpreted as effective mass m^* (Kohlfürst *et al.* 2014) which determines $\ell_{\min} = \text{int}(1 + 2m^*/\omega)$. The Fourier zero-modes as functions of p_{\perp} at $p_{\parallel} = 0$ are displayed in the bottom row in Fig. 1 together with the resonance positions. For the field “1” alone (left bottom panel) one has to take the limit $\gamma_2 \rightarrow \infty$ in the Fourier zero-mode, while field “2” alone (right bottom panel) corresponds to $\gamma_1 \rightarrow \infty$ and the replacement $\omega \rightarrow N\omega$ in (2.3).

The striking feature in Fig. 1 (cf. (Otto *et al.* 2015a,b) for other examples with different parameters, in particular $t_{\text{f.t.}}$, and (Hähnel 2015) for a wider range of field strengths) is the lifting of the spectrum related to field “1” by the assistance of field “2”. While the amplification of the created pair distribution by the assistance field can be huge, for sub-critical fields the frequency $N\omega$ must be $\mathcal{O}(m)$ to overcome the exponential suppression. This implies that intensities envisaged in ELI pillar IV (ELI 2015) must be at our disposal in conjunction with much higher frequencies to arrive at measurable pair numbers enhanced further by an assistant field (Otto *et al.* 2015b).

Even with low pair creation probability a once produced pair may seed a further

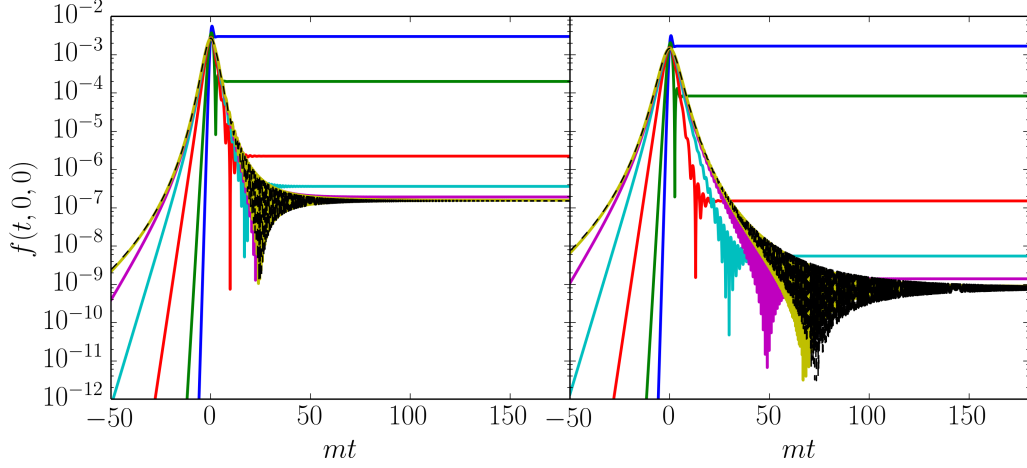


FIGURE 2. Time evolution of $f(p_{\perp} = p_{\parallel} = 0, t)$ in the adiabatic basis for the Sauter pulse (2.4) for $\tau = 1 m^{-1}$ (blue), $\tau = 2 m^{-1}$ (green), $\tau = 5 m^{-1}$ (red), $\tau = 10 m^{-1}$ (cyan), $\tau = 20 m^{-1}$ (purple), $\tau = 50 m^{-1}$ (yellow) and $E_0 = 0.2 E_c$ (left panel), $E_0 = 0.15 E_c$ (right panel). The dashed black curves depict the Schwinger case as the limit of large values of τ . Note the vast drop of the residual phase space occupancy for larger values of τ when changing E_0 from $0.2 E_c$ to $0.15 E_c$.

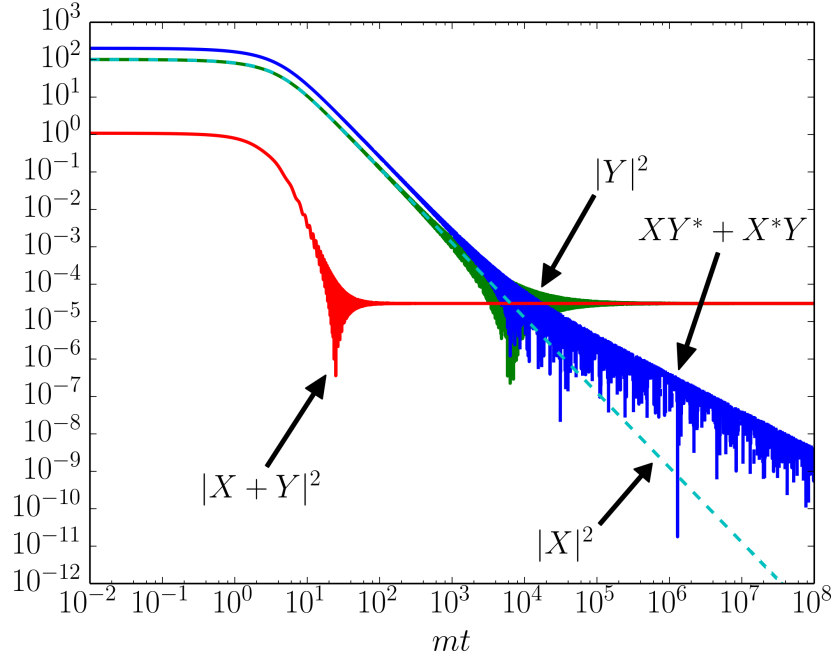


FIGURE 3. Time evolution of the components defined in (2.6) of the analytical solution (2.5) of the Schwinger case depicted for $E_0 = 0.2 E_c$. Cyan dashed curve: $|X|^2$, green curve: $|Y|^2$, blue curve: interference term $XY^* + X^*Y$, red curve: $|X + Y|^2$.

avalanche evolution (Bell & Kirk 2008; King *et al.* 2013; Elkina *et al.* 2011) toward an electron-positron plasma. In this respect one may ask for the time scales to approach the asymptotic out-state. A unique answer seems not to be achievable within the present framework due to the unavoidable ambiguity of the particle definition (see,

e.g. (Dabrowski & Dunne 2014) for examples of changing the time evolution of f at intermediate times when changing the basis). Having this disclaimer in mind one can inspect nevertheless graphs of $f(t)$. Figure 2 exhibits the time evolution in the adiabatic basis for the Sauter pulse

$$E(t) = \frac{E_0}{\cosh^2(t/\tau)}. \quad (2.4)$$

which is fairly different from (2.2). The analytical solution (Narozhny & Nikishov 1970; Hebenstreit 2011) of equation (2.1) is useful for checking numerical codes which are challenged by dealing with rapidly changing functions over many orders of magnitude. For large values of the pulse duration parameter τ the Schwinger case is recovered, see (Hebenstreit 2011):

$$f = \frac{1}{8} \left(1 + \frac{u}{\sqrt{2\hat{\eta} + u^2}} \right) e^{-\frac{\pi\hat{\eta}}{4}} |X + Y|^2 \quad (2.5)$$

with

$$X = \left(\sqrt{2\hat{\eta} + u^2} - u \right) D_{-1 + \frac{i\hat{\eta}}{2}} \left(-ue^{-\frac{i\pi}{4}} \right), \quad Y = -2e^{\frac{i\pi}{4}} D_{\frac{i\hat{\eta}}{2}} \left(-ue^{-\frac{i\pi}{4}} \right), \quad (2.6)$$

where D is the parabolic cylinder function, $u = \sqrt{\frac{2}{|e|E_0}}(p_{\parallel} + eE_0t)$ and $\hat{\eta} = \frac{m^2 + p_{\perp}^2}{|e|E_0}$. While for $E = 0.2E_c$ the net function $\propto |X + Y|^2$ reaches its asymptotic value already at $tm \approx 20$ (see Fig. 3), the individual components $|X|^2$, $|Y|^2$ and $XY^* + X^*Y$ display a violent time dependence on much longer times. Note also the subtle cancellations.

In the case of the Sauter pulse, see Fig. 2, the asymptotic values of f are reached at shorter times with decreasing values of τ . The relatively large values of $f(t \approx 0)$ have tempted sometimes researchers to relate them to particular effects caused by the transient state. Clearly, only observables, e.g. provided by probe beams, at asymptotic times are reliable. It is questionable, however, whether such probes can disentangle transient state contributions and asymptotic state contributions in a unique manner.

3. Laser assisted Breit-Wheeler process

The laser assisted, non-linear Breit-Wheeler process (cf. (Jansen & Müller 2013, 2015; Wu & Xue 2014; Krajewska & Kaminski 2014; Meuren *et al.* 2015a)) is dealt with within the strong-field QED (Furry picture) as reaction $\gamma' \rightarrow e_A^+ + e_A^-$ where e_A^{\pm} denote dressed electron/positron states as Volkov solutions of the Dirac equation in a plane wave model with vector potential of the common classical background field

$$A^{\mu}(\phi) = \gamma_X^{-1} f_X(\phi) \varepsilon_X^{\mu} \cos \phi + \gamma_L^{-1} f_L(\eta\phi) \varepsilon_L^{\mu} \cos \eta\phi, \quad (3.1)$$

where the polarization four-vectors are $\varepsilon_{X,L}^{\mu}$ and the above defined Keldysh parameters $\gamma_{1,2}$ have been transposed to $\gamma_{X,L}$; γ' denotes the high-energy probe photon traversing the field (3.1). The XFEL (frequency ω) and laser (frequency $\eta\omega$, we assume in the following $\eta \ll 1$) beams are co-propagating and their linear polarizations are set perpendicular to each other to simplify the cumbersome numerical evaluation. Both ones are pulsed as described, for the sake of computational convenience, by the envelope functions $f_X = \exp\{-\phi^2/(2\tau_X^2)\}$ and $f_L = \cos^2(\pi\phi/(2\tau_L))$ for $-\tau_L \leq \phi \leq +\tau_L$ and zero elsewhere for the latter pulse shape. In contrast to (2.2) we treat here a somewhat more realistic case with different pulse durations τ_X and τ_L . The invariant phase is $\phi = k \cdot x$ with the dot indicating the scalar product of the four-wave vector k and the space-time coordinate

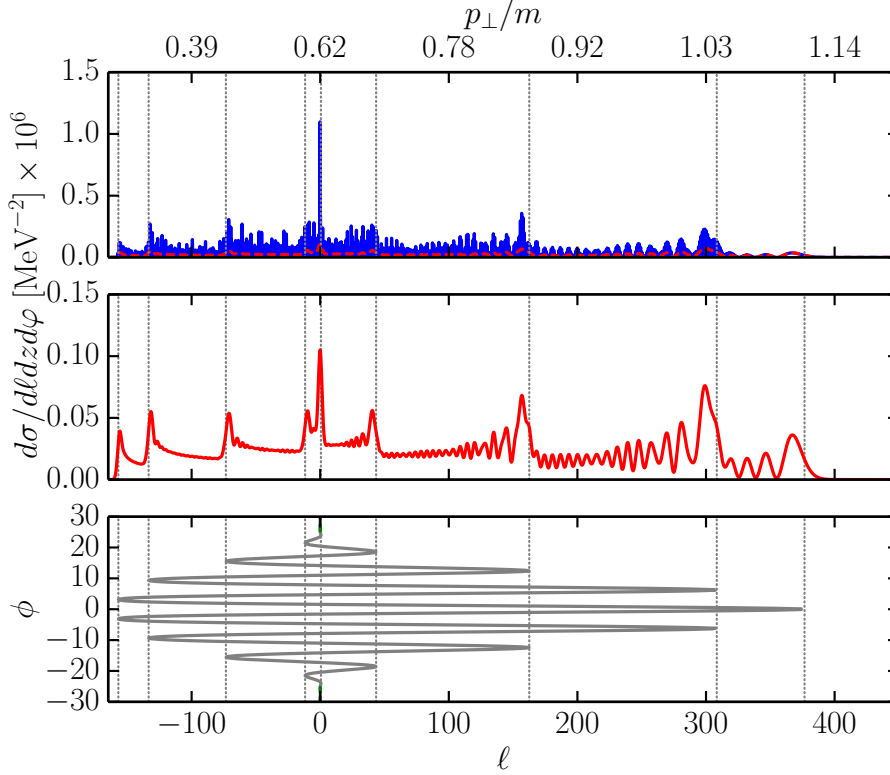


FIGURE 4. Spectra for the laser assisted Breit-Wheeler process for a probe photon of energy 60 MeV colliding head-on with an XFEL photon (energy 6 keV) and a co-propagating laser beam (frequency 10 eV). Further parameters are $\eta = 1/600$, $\gamma_X = 10^5$, $\tau_X = 7\tau/(4\pi\eta)$, $\gamma_L = 2$ and $\tau_L = 8\pi$ in the field (3.1). These parameters translate into intensities of 6.2×10^{15} W/cm² and 4.3×10^{19} W/cm² for XFEL and laser, respectively. Upper panel: $d\sigma/dldzdzd\varphi$ at $z = 0$ and $\varphi = \pi$ as a function of ℓ (lower axis; the corresponding values of p_\perp are given at the upper axis). The calculated spectrum is smoothed by a Gaussian window function with width $\delta = 1.3$ to get the red curve. Middle panel: smoothed spectrum separately. Lower panel: phase ϕ as a function of ℓ (see (Nousch *et al.* 2016) for details). The vertical dotted lines depict the positions of diverging $d\phi/d\ell$, where two branches of $\phi(\ell)$ merge.

x. It is convenient to parametrize the produced positron's phase space by the following three variables: (i) the momentum exchange parameter ℓ , (ii) the azimuthal angle φ with respect to the polarization direction of the assisting laser field and (iii) the shifted rapidity $z = \frac{1}{2} \log(p_+^+/p_+^-) + \frac{1}{2} \log((1 + \eta\ell)\omega_X/\omega_{X'})$. The energy-momentum balance for laser assisted pair production can be put into the form $k_{X'}^\mu + k_X^\mu + \ell k_L^\mu = p_+^\mu + p_-^\mu$ (μ is a Lorentz index, as above), where ℓ represents here an hitherto unspecified momentum exchange between the assisting laser field L and the produced pair. We define light-front coordinates, e.g. $x^\pm = x^0 \pm x^3$ and $\mathbf{x}_\perp = (x_1, x_2)$ and analogously the light front components of four-momenta of the probe photon X' , the XFEL photon X , the laser beam photons L and positron (subscript $+$) and electron (subscript $-$). They become handy because the laser four-momentum vectors only have one non-vanishing light-front component $k_{X,L}^- = 2\omega_{X,L}$. In particular, the energy-momentum balance contains the three conservation equations in light-front coordinates $k_{X'}^+ = p_+^+ + p_-^+$ and $\mathbf{p}_\perp^+ = -\mathbf{p}_\perp^-$. Moreover, the knowledge of all particle momenta allows to calculate ℓ via the fourth equation $\ell = ((p_+^- + p_-^- - k_{X'}^-)/k_X^- - 1)/\eta$. Treating (ℓ, z, φ) as independent variables

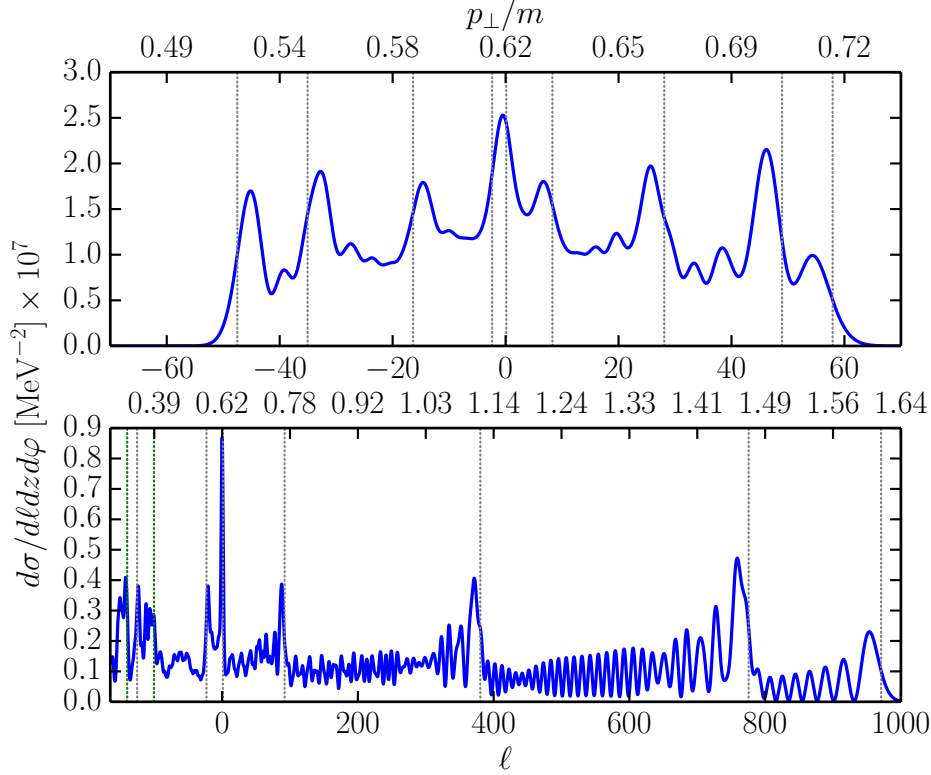


FIGURE 5. As middle panel in Fig. 4 but for $\gamma_L = 10$, laser intensity $1.7 \times 10^{18} \text{ W/cm}^2$ (top panel) and $\gamma_L = 1$, laser intensity $1.7 \times 10^{20} \text{ W/cm}^2$ (bottom panel).

the positron's four-momenta are completely determined by the above energy-momentum balance equations, see (Nusch *et al.* 2016) for details, in particular for expressing the positron and electron momenta p_{\pm} by (ℓ, z, φ) .

The theoretical basis for formulating and evaluating the cross section is outlined in (Nusch *et al.* 2016). An example is displayed in the top panel of Fig. 4 for $\eta = 1/600$, $\gamma_X = 10^5$, $\tau_X = 7\tau/(4\pi\eta)$, $\gamma_L = 2$, and $\tau_L = 8\pi$ (examples for other parameters are exhibited in (Nusch *et al.* 2016)) for kinematical conditions, where the linear Breit-Wheeler effect for $X' + X$ is just above the threshold. The involved spectral distribution (note that without the laser assistance only the Breit-Wheeler peak centered at $\ell = 0$ corresponding to $p_{\perp} = 0.62m$ would appear with a finite width as a consequence of the finite x ray pulse duration; cf. (Titov *et al.* 2012, 2013; Nusch *et al.* 2012) for an enhancement of pair production in short laser pulses). The spectrum can be smoothed by a window function with a resolution scale of $\delta = 1.3$ (which is an ad hoc choice to better show the strength distribution and which may be considered as a simple account for finite energy resolution respective p_{\perp} distribution) resulting in the red curve which is exhibited separately in the middle panel. In line with the interpretation in (Nusch *et al.* 2016; Seipt *et al.* 2015) the prominent peaks are caustics related to stationary phase points determined by the turning points of the invariant phase ϕ as a function of the variable ℓ , see bottom panel. This interpretation implies that the total cross section may be approximately factorized into a plain Breit-Wheeler production part and a final-state interaction part, where the latter one means the redistribution of the produced particles by the impact of the laser field. An analog interpretation of particle production in con-

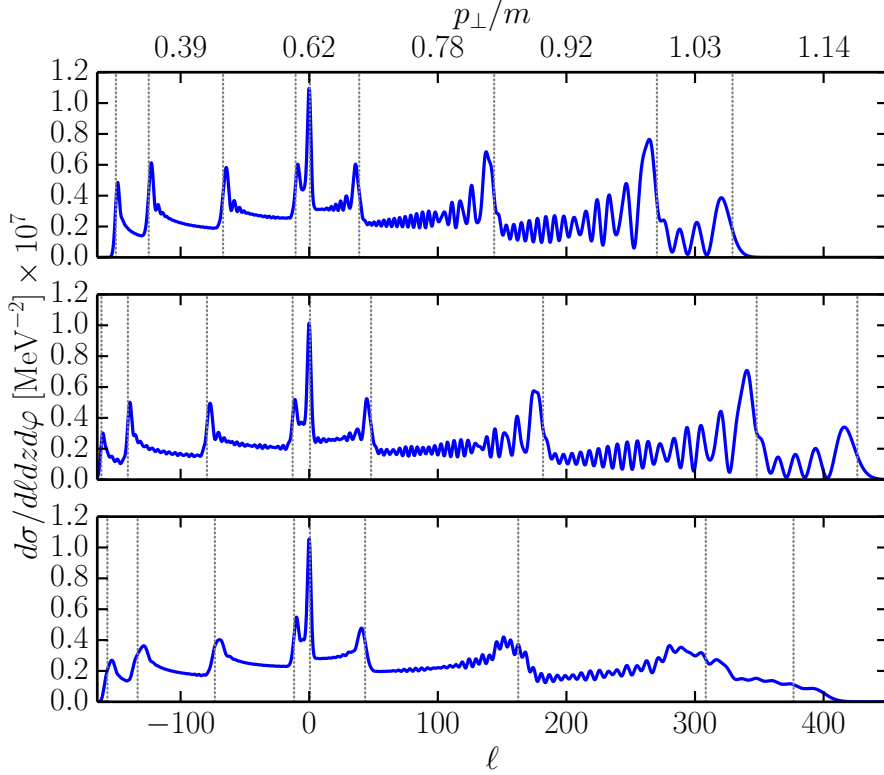


FIGURE 6. As middle panel in Fig. 4 but variation of γ_L around $\gamma_L = 2$. Upper panel: $\gamma_L = 2.22$, middle panel: $\gamma_L = 1.82$, lower panel: superposition of smoothed spectra for $\gamma_L = 1.88 \dots 2.12$ corresponding to the laser intensity parameter $a_0 = \gamma_L^{-1} = 0.5 \pm 0.03$.

stant cross field approximation in very strong fields have been put forward in (Meuren *et al.* 2015b). Figure 5 demonstrates the strong impact of the laser field intensity. For smaller values of γ_L , the transverse momentum spectrum becomes more stretched and its shape is changed. This challenges the observability of the peaks related to caustics in multi-shot experiments with fluctuating laser intensities. In fact, for the unfavorable case of equally weighted deviations, a window of less than 20% is required to keep the peak structures, see Fig. 6. A truncated Gaussian distribution with 1σ width in the same interval is, of course, much more favorable for keeping the peaks, in particular for larger p_\perp . We consider here only one particular case of the laser assisted, linear Breit-Wheeler process which turns into the textbook Breit-Wheeler process upon switching off the laser. Non-linearities w.r.t. the XFEL beam, subthreshold (w.r.t. the $X' + \text{XFEL}$ kinematics) effects combined with larger laser intensities, carrier envelope phase effects, and a wider range of kinematical parameters (e.g. $\omega_L = \mathcal{O}(1 \text{ eV})$) need to be explored as well to arrive at a complete picture. Among the furthermore to be analyzed issues w.r.t. an experimental proposal are non-monochromaticity and misalignment disturbances.

4. Summary

In summary we have supplied further important details of (i) the amplification effect of the assisted dynamical Schwinger effect and (ii) the phase space redistribution in the laser assisted Breit-Wheeler process. Both topics are motivated by the availability of x

rays by XFELs and upcoming ultra-high intensity laser beams. We consider the perspectives offered by the combination of both beam types resulting in bi-frequent fields. Concerning the Schwinger related investigations we find that significant pair production by the dynamical assistance requires much higher frequencies than such ones provided by XFEL beams in conjunction with future ELI-IV field intensities. The crucial challenge for the laser assisted Breit-Wheeler process and an access to the predicted caustic structures is the high-energy probe photon beam in combination with dedicated phase space selective detector set-ups. The bi-frequent fields are dealt with as a classical background. An avenue for further work is the proper account of quantum fluctuations and a unifying description of counter- and co-propagating fields.

Acknowledgements R. Sauerbrey, T. E. Cowan and H. Takabe are thanked for the collaboration within the HIBEF project (HIBEF 2015). D.B. and S.A.S. acknowledge support by NCN under grant number UMO-2014/15/B/ST2/03752.

Dedicated to the memory of Nikolay Borisovich Narozhny who pioneered this field of research.

REFERENCES

- AKAL, I., VILLALBA-CHÁVEZ, S. & MÜLLER, C. 2014 Electron-positron pair production in a bifrequent oscillating electric field. *Phys. Rev. D* **90**, 113004.
- AUGUSTIN, S. & MÜLLER, C. 2014 Nonlinear Bethe-Heitler Pair Creation in an Intense Two-Mode Laser Field. *J. Phys.: Conf. Ser.* **497** (1), 012020.
- BAMBER, C. *et al.* 1999 Studies of nonlinear QED in collisions of 46.6-GeV electrons with intense laser pulses. *Phys. Rev. D* **60**, 092004.
- BELL, A. & KIRK, J. 2008 Possibility of Prolific Pair Production with High-Power Lasers. *Phys. Rev. Lett.* **101** (20), 200403.
- BIALYNICKI-BIRULA, I., GORNICKI, P. & RAFELSKI, J. 1991 Phase space structure of the Dirac vacuum. *Phys. Rev. D* **44**, 1825–1835.
- BREIT, G. & WHEELER, J. A. 1934 Collision of Two Light Quanta. *Phys. Rev.* **46**, 1087.
- BREZIN, E. & ITZYKSON, C. 1970 Pair Production in Vacuum by an Alternating Field. *Phys. Rev. D* **2** (7), 1191–1199.
- BURKE, D. L. *et al.* 1997 Positron Production in Multiphoton Light-by-Light Scattering. *Phys. Rev. Lett.* **79**, 1626–1629.
- DABROWSKI, R. & DUNNE, G. V. 2014 Superadiabatic particle number in Schwinger and de Sitter particle production. *Phys. Rev. D* **90** (2), 025021.
- DI PIAZZA, A., LÖTSTEDT, E., MILSTEIN, A. I. & KEITEL, C. H. 2010 Effect of a strong laser field on electron-positron photoproduction by relativistic nuclei. *Phys. Rev. A* **81** (6).
- DI PIAZZA, A., MÜLLER, C., HATSAGORTSYAN, K. Z. & KEITEL, C. H. 2012 Extremely high-intensity laser interactions with fundamental quantum systems. *Rev. Mod. Phys.* **84** (3), 1177–1228.
- DUNNE, G. V., GIES, H. & SCHÜTZHOLD, R. 2009 Catalysis of Schwinger vacuum pair production. *Phys. Rev. D* **80** (11), 111301.
- ELI 2015 European Extreme Light Infrastructure (ELI). www.eli-laser.eu.
- ELKINA, N. V., FEDOTOV, A. M., KOSTYUKOV, I. YU., LEGKOV, M. V., NAROZHNY, N. B., NERUSH, E. N. & RUHL, H. 2011 QED cascades induced by circularly polarized laser fields. *Phys. Rev. ST Accel. Beams* **14** (5), 054401.
- GELIS, F. & TANJI, N. 2013 Formulation of the Schwinger mechanism in classical statistical field theory. *Phys. Rev. D* **87** (12), 125035.
- GELIS, F. & TANJI, N. 2015 Schwinger mechanism revisited. *arXiv:1510.05451*.
- HÄHNEL, S. 2015 Paarerzeugung in elektrischen Feldern: Numerische Untersuchungen zum Schwinger-Effekt. Bachelor's thesis, Technische Universität Dresden.
- HEBENSTREIT, F. 2011 Schwinger effect in inhomogeneous electric fields. PhD thesis, Karl-Franzens-Universität Graz.

- HEBENSTREIT, F. & FILLION-GOURDEAU, F. 2014 Optimization of Schwinger pair production in colliding laser pulses. *Phys. Lett. B* **739**, 189–195.
- HEINZ, S. *et al.* 2000 Positron spectra from internal pair conversion observed in U-238 + Ta-181 collisions. *Eur. Phys. J. A* **9**, 55–61.
- HIBEF 2015 The HIBEF project. www.hzdr.de/hgfbeamline.
- HiPER 2015 High Power laser for Energy Research project (HiPER). www.hiper-laser.org.
- JANSEN, M. J. A. & MÜLLER, C. 2013 Strongly enhanced pair production in combined high- and low-frequency laser fields. *Phys. Rev. A* **88** (5), 052125.
- JANSEN, M. J. A. & MÜLLER, C. 2015 Strong-Field Breit-Wheeler Pair Production in Short Laser Pulses: Identifying Multiphoton Interference and Carrier-Envelope Phase Effects. *arXiv:1511.07660* .
- KING, B., ELKINA, N. & RUHL, H. 2013 Photon polarisation in electron-seeded pair-creation cascades. *Phys. Rev. A* **87**, 042117.
- KOHLFÜRST, C., GIES, H. & ALKOFER, R. 2014 Effective Mass Signatures in Multiphoton Pair Production. *Phys. Rev. Lett.* **112** (5), 050402.
- KOHLFÜRST, C., MITTER, M., VON WINCKEL, G., HEBENSTREIT, F. & ALKOFER, R. 2013 Optimizing the pulse shape for Schwinger pair production. *Phys. Rev. D* **88** (4), 045028.
- KRAJEWSKA, K. & KAMINSKI, J. Z. 2014 Breit-Wheeler pair creation by finite laser pulses. *J. Phys. Conf. Ser.* **497**, 012016.
- MEUREN, S., HATSAGORTSYAN, K. Z., KEITEL, C. H. & DI PIAZZA, A. 2015*a* Polarization-operator approach to pair creation in short laser pulses. *Phys. Rev. D* **91** (1), 013009.
- MEUREN, S., KEITEL, C. H. & DI PIAZZA, A. 2015*b* Semiclassical description of nonlinear electron-positron photoproduction in strong laser fields. *arXiv:1503.03271* .
- MÜLLER, B., PEITZ, H., RAFELSKI, J. & GREINER, W. 1972 Solution of the Dirac equation for strong external fields. *Phys. Rev. Lett.* **28**, 1235.
- MÜLLER, B., RAFELSKI, J. & GREINER, W. 1973 Solution of the Dirac equation with two Coulomb centers. *Phys. Lett. B* **47**, 5–7.
- NAROZHNY, N. B., BULANOV, S. S., MUR, V. D. & POPOV, V. S. 2004 e^+e^- -pair production by a focused laser pulse in vacuum. *Phys. Lett. A* **330** (1-2), 1–6.
- NAROZHNY, N. B. & NIKISHOV, A. I. 1970 The simplest processes in the pair creating electric field. *Sov. J. Nucl. Phys.* **11**, 596.
- NOUSCH, T., SEIPT, D., KÄMPFER, B. & TITOV, A. I. 2012 Pair production in short laser pulses near threshold. *Phys. Lett. B* **715** (1–3), 246–250.
- NOUSCH, T., SEIPT, D., KÄMPFER, B. & TITOV, A. I. 2016 Spectral caustics in laser assisted Breit–Wheeler process. *Phys. Lett. B* .
- OTTO, A., SEIPT, D., BLASCHKE, D., KÄMPFER, B. & SMOLYANSKY, S. A. 2015*a* Lifting shell structures in the dynamically assisted Schwinger effect in periodic fields. *Phys. Lett. B* **740**, 335–340.
- OTTO, A., SEIPT, D., BLASCHKE, D. B., SMOLYANSKY, S. A. & KÄMPFER, B. 2015*b* Dynamical Schwinger process in a bifrequent electric field of finite duration: Survey on amplification. *Phys. Rev. D* **91** (10), 105018.
- PANFEROV, A. D., SMOLYANSKY, S. A., OTTO, A., KÄMPFER, B., BLASCHKE, D. B. & JUCHNOWSKI, L. 2015 Assisted dynamical Schwinger effect: pair production in a pulsed bifrequent field. *arXiv:1509.02901* .
- RAFELSKI, J., FULCHER, L. P. & GREINER, W. 1971 Superheavy elements and an upper limit to the electric field strength. *Phys. Rev. Lett.* **27**, 958–961.
- RAFELSKI, J., MÜLLER, B. & GREINER, W. 1978 Spontaneous vacuum decay of supercritical nuclear composites. *Zeitschrift für Physik A Atoms and Nuclei* **285** (1), 49.
- SAUTER, F. 1931 Über das Verhalten eines Elektrons im homogenen elektrischen Feld nach der relativistischen Theorie Diracs. *Z. Physik.* **69** (11), 742.
- SCHMIDT, S. M., BLASCHKE, D. B., RÖPKE, G., SMOLYANSKY, S. A., PROZORKEVICH, A. V. & TONEEV, V. D. 1998 A Quantum kinetic equation for particle production in the Schwinger mechanism. *Int. J. Mod. Phys. E* **7**, 709.
- SCHÜTZHOLD, R., GIES, H. & DUNNE, G. 2008 Dynamically Assisted Schwinger Mechanism. *Phys. Rev. Lett.* **101** (13), 130404.
- SCHWINGER, J. 1951 On Gauge Invariance and Vacuum Polarization. *Phys. Rev.* **82**, 664.

- SEIPT, D., SURZHYKOV, A., FRITZSCHE, S. & KÄMPFER, B. 2015 Caustic structures in the spectrum of x-ray Compton scattering off electrons driven by a short intense laser pulse. *arXiv:1507.08868* .
- TITOV, A. I., KÄMPFER, B., TAKABE, H. & HOSAKA, A. 2013 Breit-Wheeler process in very short electromagnetic pulses. *Phys. Rev. A* **87**, 042106.
- TITOV, A. I., TAKABE, H., KÄMPFER, B. & HOSAKA, A. 2012 Enhanced Subthreshold e^+e^- Production in Short Laser Pulses. *Phys. Rev. Lett.* **108**, 240406.
- WU, Y. B. & XUE, S. S. 2014 Nonlinear Breit-Wheeler process in the collision of a photon with two plane waves. *Phys. Rev. D* **90** (1), 013009.
- ZOU, J. P. *et al.* 2015 Design and current progress of the Apollon 10 PW project. *HPLaser* **3**.